Pure & Appl. Chem., Vol. 60, No. 8, pp. 1123–1132, 1988.
Printed in Great Britain.

Characteristics of electron transfer reactions of early transition elements

Kazuo SAITO* and Yoichi SASAKI**

Coordination Chemistry Laboratories, Institute for Molecular Science, Okazaki 444, Japan and Chemistry Department, Faculty of Science, Tohoku University, Sendai 980, Japan**

Abstract —— This article consists of three parts. First is related to the structural and kinetic studies of electron transfer in oxovanadium(IV) and dioxovanadium(V) complexes. The oxidation of VO^{2+} complexes is discussed with reference to the formation of second oxo-ligand at the cis-site of V=O. Second is the electrochemistry of bi- and ternuclear species of molybdenum and tungsten and their mixed metal complexes with bridging oxide. A gradual change of the electrode potential was observed among them with given structure. Third is the studies of crystal structure and redox potential of octahedral hexanuclear molybdenum complexes of mixed capping ligands with halide and chalcogenide. The ease of electron transfer remarkably changes on the replacement of capping halide by sulfide or selenide, although the change in bond distances is very modest.

INTRODUCTION

High valent ions of early transition elements have strong affinity towards oxide ions and very often give oxo-anions. When the overall charge of the oxo-ions remains positive, one or more oxide ions form strong and inert bond with the metal ions to give such ions as $V^{IV}O^{2+}$, $V^{V}O_2^{+}$, $Mo^{VI}O_2^{2+}$ and $Mo^{V}O^{3+}$. Two oxide ions occupy generally cis positions to each other with small numbers of exceptions such as UO_2^{2+}. The ligand substitution reaction exhibits a remarkable regio-selectivity; the cis-site (basal site) is much more inert than the trans-site (apical site). We want to demonstrate that such a regio-selectivity is also revealed on electron transfer processes.

Another characteristics of early transition elements is to form bi- or multi-nuclear complexes with or without metal-metal bond. Binuclear species with $[M^{V}{}_2(\mu_2\text{-}O)_2O_2]^{2+}$ core and ternuclear species with $[M^{IV}{}_3(\mu_2\text{-}O)_3(\mu_3\text{-}O)]^{4+}$ or $[M^{IV}{}_3(\mu_3\text{-}O)_2]^{8+}$ core give mixed metal complexes with M = Mo and W. Their electron transfer reactions are quite characteristic of the structure, the metal ions and the connecting ligands. Octahedral hexa-metal clusters are well known in the form of e.g. face capped $[M_6X_8]^{4+}$ or edge-bridged $[M_6X_{12}]$ (X = halide) but little is known of their redox behaviour in solution and the existence of mixed capping ligand species.

We have studied these characteristic behaviour both kinetically and electrochemically with special reference to the relationship between their structure and properties.

REDOX CHARACTERISTICS OF OXOVANADIUM COMPLEXES

Oxovanadium(IV) complexes exhibit remarkable regio-selectivity on ligand substitution (ref. 1 to 4), and the electron transfer reactions are also very special. Dimerization with bridging oxide between vanadium(IV) and vanadium(V) at the basal site provides mixed valence species with $V_2O_3^{3+}$core (Fig. 1, ref. 5), whereas that at the apical site gives distinguished V^{IV} and V^{V} central ions. (ref. 6) Formation of the mixed valence complex was demonstrated not only in crystalline state, but also in solution. (ref. 5)

* Present address: Natural Science Building, International Christian University, Osawa, Mitaka, Tokyo 181, Japan.

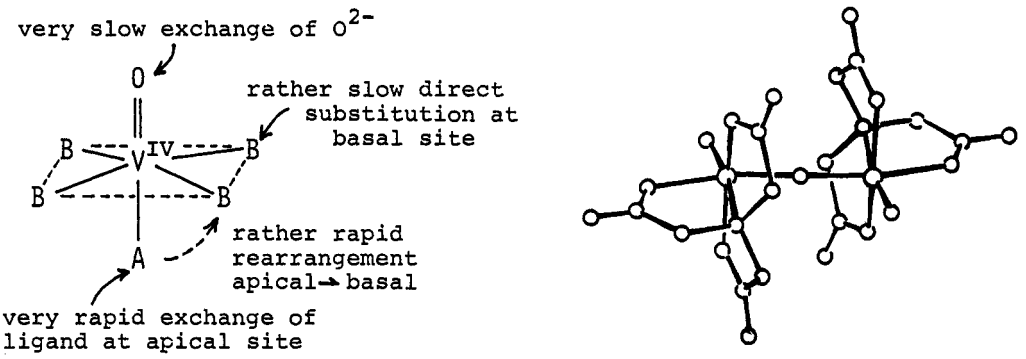

Fig. 1 Structure and characteristics of oxovanadium complexes. left, approximate ligand substitution rate of $V^{IV}O^{2+}$ species. right, structure of the mixed valence binuclear complex with $V_2O_3^{3+}$ core, $(NH_4)_3[(nta)V(=O)OV(=O)(nta)].3H_2O$, $C2/c$ symmetry.

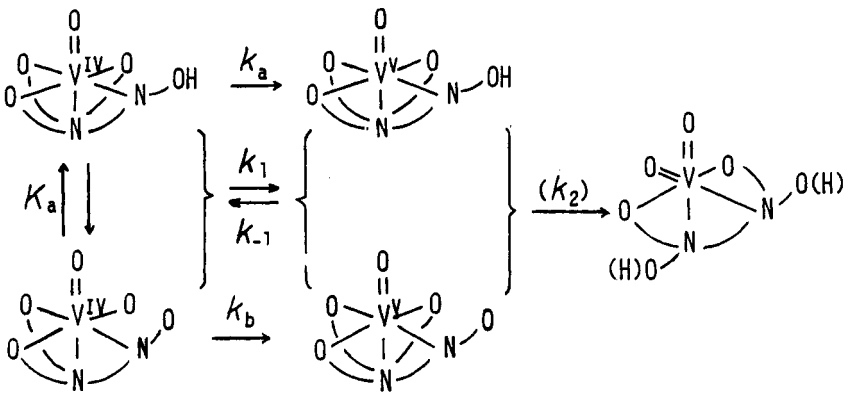

Fig. 2 Reaction scheme of the oxidation of $[V^{IV}O(edta)]^{2-}$ with hexachloroiridate in aqueous solution of pH 3 to 4.5

TABLE 1. pH Dependence of the kinetic data for the oxidation of $[V^{IV}O(EDTA)]$ with $[Ir^{IV}Cl_6]^{2-}$ analysed by Eqs. 3 and 4.

pH	3.15	3.25	3.50	4.25
$k_1/10^2M^{-1}s^{-1}$	4.7 ± 0.6	5.0 ±0.9	5.4 ± 1.1	6.1 ± 1.3
$(k_2/k_{-1})/10^{-4}M$	1.1 ± 0.3	1.3 ± 0.2	1.7 ± 0.4	3.0 ± 0.7

25°C, I = 1.0 M($NaClO_4$), acetate buffer (0.10 M), $[V^{IV}O(EDTA)]_{total}$ = (3.55 ∿ 12.0) x 10^{-3} M

TABLE 2. Kinetic data for the oxidation of $[V^{IV}O(edtaH)]^-$ (k_a) and $[V^{IV}O(edta)]^{2-}$ (k_b) in water.

	$k/M^{-1}s^{-1}$	$\Delta H^{\ddagger}$/kJ mol^{-1}	$\Delta S^{\ddagger}$/J $mol^{-1}K^{-1}$
k_a	3.3 x 10^2	55.0 ± 2.2	-13 ± 7
k_b	6.5 x 10^2	58 ± 18	+1 ± 70

at 25°C, I = 0.1 M($NaClO_4$), 0.10 M acetate buffer, oxidant, $[Ir^{IV}Cl_6]^{2-}$

Structural requirement for the oxidation of VO^{2+} to $V^{V}O_2^{+}$

Vanadium(V) is present in aqueous solution of pH < 4 as *cis*-dioxo ions VO_2^{+} and oxidation of $V^{IV}O^{2+}$ complexes is accompanied by the formation of another V=O bond at the basal site. This fact was clearly demonstrated by the oxidation of $[V^{IV}O(edta)]^{2-}$ with hexachloroiridate(IV) $[Ir^{IV}Cl_6]^{2-}$ in aqueous solution. (ref. 7) (Note a) EDTA coordinates as quinquedentate to oxovanadium(IV), and as quadridentate to dioxovanadium(V) as shown in Fig. 2. (ref. 8) Alkalimetric titration of $[V^{IV}O(edtaH)]^{-}$ gives only one inflection at pH < 11, and there was no change in electronic spectrum at pH 2.5 to 6.7 indicating that the deprotonation takes place at a remote site from the vanadium(IV), i.e. at the free acetate branch. If there were coordinated water molecule, another inflection should be found at pH 6 to 9. The free acetate should be branched from the nitrogen atom at the basal site, since meridional coordination of an iminodiacetate moiety is sterically more difficult. Structure of the product was determined by the X-ray method.

The rate of the overall redox reaction is greater by two orders than that of the ligand substitution reactions of the oxidant and reductant. Kinetic studies were performed in the presence of excessive reductant by the spectrophotmetric method at 487 nm (peak of $[Ir^{IV}Cl_6]^{2-}$) under varying concentrations of the oxidant, reductant, and $[Ir^{III}Cl_6]^{3-}$ at pH 3.15 to 4.35. The results are summerized in Fig. 2 and Tables 1 and 2.

The observed first order rate constant with respect to the oxidant depends linearly on the concentration of $[V^{IV}O(EDTA]$ at a given concentration of $[Ir^{III}Cl_6]^{3-}$ and pH. The ratio $[V^{IV}O(EDTA)]/k_{obs}$ has a good linear relation with $[Ir^{III}Cl_6{}^{3-}]$ at a given pH, and hence k_{obs} is expressed by Eq. 1.

$$k_{obs} = p[V^{IV}O]/(q[Ir^{III}] + r) \quad (1)$$

The dependence of k_{obs} upon $[Ir^{III}Cl_6{}^{3-}]$ suggests the presence of a reactive intermediate, most probably monoxovanadium(V)-EDTA complex with a similar structure to that of the original $[V^{IV}O(EDTA)]$. Thus the mechanism given in Fig. 2 is consistent with the rate law of Eq. 1 at a given pH. Application of the steady-state approximation to the intermediate $[V^{V}O(EDTA)]$ gives Eq.2.

$$-\frac{d[Ir^{IV}]}{dt} = \frac{k_1 k_2 [V^{IV}][Ir^{IV}]}{k_{-1}[Ir^{III}] + k_2} \quad (2)$$

This form is equal to Eq. 1, and k_{obs} is expressed by Eq. 3 and hence Eq. 4.

$$k_{obs} = k_1 k_2 [V^{IV}]/(k_{-1}[Ir^{III}] + k_2) \quad (3)$$

$$\frac{[V^{IV}]}{k_{obs}[Ir^{III}]} = \frac{k_{-1}}{k_1 k_2} + \frac{1}{k_1[Ir^{III}]} \quad (4)$$

The plot of $[V^{IV}][Ir^{III}]^{-1}k_{obs}{}^{-1}$ vs. $[Ir^{III}]^{-1}$ gives k_1 and k_2/k_{-1} on the slope and intercept, respectively. The dependence of k_1 on pH was analysed by use of the pK_a values of $[V^{IV}O(edtaH)]^{-}$ (Fig. 2) and Eq. 5 was obtained.

$$k_1 = (k_a[H^+] + k_b K_a)/([H^+] + K_a) \quad (5)$$

The plot of $k_1([H^+] + K_a)$ vs. $[H^+]$ gives a straight line and k_a and k_b are calculated as shown in Table 2.

The observed k_{obs} values are much smaller than those of similar oxidation of $[V^{IV}O(nta)(H_2O)]^{-}$ and $[V^{IV}O(pmida)(H_2O)]$ with $[Ir^{IV}Cl_6]^{2-}$. This is due to the contribution of small k_2/k_{-1} values. When the results were analysed as shown above, the k_a and k_b values are of the same order of those of the other two complexes. The electron transfer itself from V^{IV} to Ir^{IV} should proceed in a similar manner to those of these complexes, and the protonation at the remote site affects the rate of electron transfer little. We can thus make clear that the oxidation of $[V^{IV}O(EDTA)]$ with $[Ir^{IV}Cl_6]^{2-}$ has two steps, and the second is the formation of oxo ligand at the basal site.

Note a: edta, ethylenediamine-*N*,*N*,*N*',*N*'-tetraacetate(4-) ion; EDTA, inclusive sign for variously protonated species of $edta^{4-}$; nta, nitrilotriacetate(3-) ion; pmida, 2-pyridylmethyiminodiacetate ion; pida, phosphonomethyliminodiacetate(4-) ion; en. ethylenediamine.

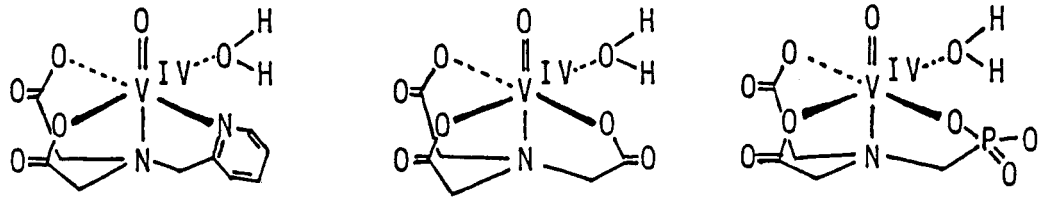

$[V^{IV}O(pmida)(H_2O)]$ $[V^{IV}O(nta)(H_2O)]^-$ $[V^{IV}O(pida)(H_2O)]^{2-}$

Fig. 3 Structure of *cis*-aquaoxo-quadridentatovanadium(IV) complexes. (abreviation of ligands *cf.* Note a)

Difference between aqua and hydroxo complexes

Oxovanadium(IV) complexes with the quadridentate ligands (quad), pmida, nta, and pida have aqua ligand at the basal site, and the coordinated water molecules are deprotonated with pK_a values 6.4, 6.9 and 8.4 at 25°C and I = 1.0 M ($NaClO_4$), respectively. The large pK_a of the pida complex (ref. 9) is due to the hydrogen bond between water and phosphonate branch of $pida^{4-}$. All these complexes are oxidized with $[Ir^{IV}Cl_6]^{2-}$ and binuclear $[(en)_2Co^{III}(\mu\text{-}NH_2,\mu\text{-}O_2^{(-)})Co^{III}(en)_2]^{4+}$ to the corresponding $[V^{V}O_2(quad)]$ complexes. The rates are much greater than those of their ligand substitution reactions and depend on the pH from 4 to 7. The results with iridate(IV) as oxidant are summerized by Eq. 6 and the data analyzed by Eq. 7.

$$\begin{array}{lcl} [V^{IV}O(quad)(H_2O)]^{n-} & + [Ir^{IV}Cl_6]^{2-} \xrightarrow{k_{H_2O}} & \text{product} \\ \uparrow K_a \downarrow & & \\ [V^{IV}O(quad)(OH)]^{(n+1)-} & + [Ir^{IV}Cl_6]^{2-} \xrightarrow{k_{OH}} & \text{product} \end{array} \quad (6)$$

$$-d[Ir^{IV}]/dt = (k_{H_2O} + k_{OH}K_a[H^+]^{-1})[V^{IV}][Ir^{IV}] \quad (7)$$

When the rate was followed by the measurement of extinction at 487 and 690 nm (peaks of the oxidants), the observed first order rate constant is expressed by Eq. 8.

$$k_{obs} = (k_{H_2O} + k_{OH}K_a[H^+]^{-1})[V^{IV}] \quad (8)$$

Kinetics of oxidation with the Co^{III} complex is more complicated because the high charges of V^{IV} and Co^{III} complexes with opposite sign lead to ion pairs (IP) which act as precursor of oxidation. (Eq. 9)

$$\begin{array}{lcl} [V^{IV}O(quad)(H_2O)]^{n-} + [\mu\text{-}O_2]^{4+} \rightleftharpoons^{K_{os}} (IP) \xrightarrow{k_e} & \text{product} \\ \uparrow\downarrow K_a & \\ [V^{IV}O(quad)(OH)]^{(n+1)-} + [\mu\text{-}O_2]^{4+} \rightleftharpoons^{K_{os}} (IP) \xrightarrow{k_e} & \text{product} \end{array} \quad (9)$$

The rate is expressed by Eq. 10, and individual values of K_{os}, K'_{os}, k_e and k'_e are obtained from the first order rate constants at varying conditions.

$$k_{obs} = (k_eK_{os} + k'_eK'_{os}K_a[H^+]^{-1})[V^{IV}]/\{1 + (K_{os} + K'_{os}K_a[H^+]^{-1}\}[V^{IV}] \quad (10)$$

The results are summerized in Table 3. Since the individual results were reported elsewhere (ref. 10), they are compared with one another with reference to the activation parameters. There is a remarkable difference between the rates of aqua and hydroxo complexes. The aqua complex with pida gives an intermediate value; this is because the hydrogen-bonded complex can be reckoned as in an intermediate state between aqua and hydroxo.

One might consider that the aqua complexes are oxidized with more difficulty because the difference in V-O distance between aqua and oxo is greater than that between hydroxo and oxo, and the Franck-Condon reorganization energy is larger. If this interpretation were appropriate, the difference in rate should be reflected in $\Delta H^{\ddagger}$ values (ref. 11). The difference in $\Delta H^{\ddagger}$ is rather modest between aqua and hydroxo complexes. When $\Delta H^{\ddagger}$ is plotted against the charge product of oxidant and reductant, all the values are on a straight line. (Fig. 4) Change in the charge product will represent the association of the redox pair to give the precursor. There seems to be no substantial difference in the ease of electron transfer between the aqua and hydroxo complexes on Franck-Co don basis. On the other hand, a similar plot of $\Delta S^{\ddagger}$ gives a significant difference. The observed k_e of a single electron

TABLE 3 Rate of oxidation of $[V^{IV}O(\text{quadridentate})(H_2O)]$ and $[V^{IV}O(\text{quadridentate})(OH)]$ by hexachloroiridate(IV)

Complexes	$k_2/M^{-1}s^{-1}$	$\Delta H^{\ddagger}$/kJ mol^{-1}	$\Delta S^{\ddagger}$/J mol^{-1}K^{-1}
$[V^{IV}O(\text{pmida})(H_2O)]$	9.1×10^2	52 ± 8	-8 ± 38
$[V^{IV}O(\text{nta})(H_2O)]^-$	1.4×10^2	46 ± 8	-46 ± 17
$[V^{IV}O(\text{pidaH})(H_2O)]^-$	7×10^2	—	—
$[V^{IV}O(\text{pmida})(OH)]^-$	2.9×10^6	42 ± 1	+21 ± 2
$[V^{IV}O(\text{nta})(OH)]^{2-}$	1.4×10^6	37 ± 3	-2 ± 8
$[V^{IV}O(\text{pida})(OH)]^{2-}$	1.1×10^4	29 ± 3	-65 ± 11

at 25°C, I = 0.1 M ($NaClO_4$)

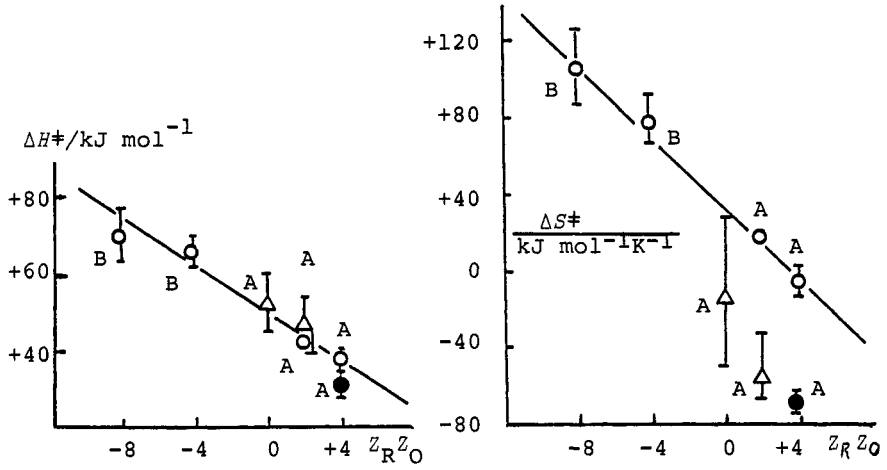

Fig. 4 Relationship between activation parameters and charge product for the redox couples at I = 0.1 M in water. reductants $[V^{IV}O(\text{quad})(OH)]$ (o), $[V^{IV}O(\text{quad})(H_2O)]$ (Δ) and $[V^{IV}O(\text{pida})(H_2O)]$ (●); oxidant A, $[Ir^{IV}Cl_6]^{2-}$, B, binuclear cobalt(III) complex.

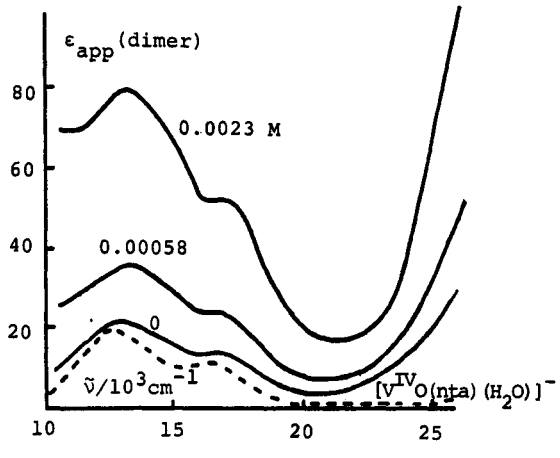

Fig. 5 Absoprtion spectra in miceller solution. $Na_3[V_2O_3(\text{nta})_2]$ in acetate buffer at 25°C, [CTAB]/10^{-4}M

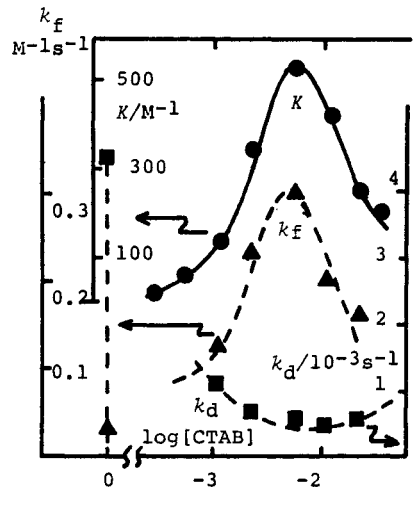

Fig. 6 Change in forward (k_f) and backward (k_d) reaction rate and the equilibrium constant with change in CTAB concn.

transfer process is expressed by Eq. 11, where κ_{el}, T, k_B, $\Delta G_\lambda^{\ddagger}$ and R are the electronic transmission coefficient, absolute temperature, Bolzmann constant, Franck-Condon reorganization energy and gas constant, respectively.

$$k_e = \kappa_{el} k_B T \exp(\Delta G_\lambda^{\ddagger}/RT)/h \qquad (11)$$

When the electron transfer involves a non-adiabatic process, a small κ_{el} is expected, which may bring forward a more negative entropy of activation, but be not reflected in enthalpy of activation. Discussion on non-adiabaticity of an electron transfer process may be further cultivated by introducing the volume of activation, but the details will be discussed elsewhere. (ref. 12)

Influence of the environment

We have shown that the following equilibrium is established in aqueous solution, when $V^{IV}O^{2+}$ and $V^{V}O_2^{+}$ complexes of a given quadridentate are mixed.

$$[VO(quad)(H_2O)]^{n-} + [VO_2(quad)]^{(n+1)-} \overset{K}{\rightleftharpoons} [(quad)\overset{O}{\overset{\|}{V}}\text{-O-}\overset{O}{\overset{\|}{V}}(quad)]^{(2n+1)-} \qquad (12)$$

The product has a deep blue color, and the equivalence of two vanadium atoms was demonstrated by the equal V-O-V distance in crystals, and by appearance of 15 hyperfine ESR peaks in chilled solution. (ref. 5) The equilibrium constant is 20 M^{-1} at 25°C and I = 1.0 M. Since the rightward reaction involves association of two anions, the K value should be affected by the environment of the solution. The influence of ionic strength, counter ions and the solvent provides useful information, but the influence of micelles is very remarkable.

Figure 5 shows the change in absorption spectrum on addition of the cationic surfactant cetyltrimethylammonium bromide CTAB. Increase in extinction shows the increase in concentration of the binuclear species, and hence the shift of equilibrium to the right. Figure 6 shows the change of rate constants right (k_f) and leftward (k_d) and K with increase in CTAB concentration. Clear peaks are seen near the critical micelle concentration. The maximum K value was 800 M^{-1} at [CTAB] = 0.0023 M and [complex] = 0.0004 M. The change in k_d is very modest.

BI- AND TERNUCLEAR SPECIES BRIDGED BY OXIDE IONS

Early transition elements tend to form bi- and multi-nuclear complexes bridged by oxide. Figure 7 shows examples of binuclear molybdenum(V) and ternuclear molybdenum(IV) complexes. We have demonstrated that the oxidation of one Mo^{V} to Mo^{VI} in the $Mo^{V}_2O_4^{2+}$ complexes is the rate determining step, and this process takes place by the outer-sphere mechanism. (ref. 13) When the $Mo^{V}_2O_4^{2+}$ complex was optically active (e.g. with R-propylediamine-N,N,N',N'-tetraacetate in place of edta), oxidation with the asymmetric binuclear cobalt(III) complex $\Delta\Delta$-$[(en)_2Co^{III}(\mu\text{-}NH_2,\mu\text{-}O_2^{(-)})Co^{III}(en)_2]^{4+}$ involved stereoselectivity. (ref. 14) In the presence of optically active Λ-$[Co^{III}(en)_3]^{3+}$ the oxidation of $[Mo^{V}_2O_4(R,S\text{-pdta})]^{2-}$ with $[Ir^{IV}Cl_6]^{2-}$ also involved stereoselectivity. (ref. 15) We discussed the importance of ionic association of the redox pairs to form the precursor (with optically active counter ion as mediator in the latter case) as source of selectivity.

Not only molybdenum but also tungsten form bi- and ter-nuclear complexes with similar structures in W^{V} and W^{IV} state. (ref. 16) A mixed metal complex $[Mo^{V}W^{V}O_4(edta)]^{2-}$ was synthesized in crystalline state (ref. 17), and the electrode potentials of $[M^{V}_2O_4(edta)]^{2-}$ type complexes measured. (Table 4) The E values are subject to rather significant change depending on pH and buffer ions, and the discussion should remain qualitative. However, the substitution of tungsten for molybdenum decreases the potential of both one electron oxidation to M^{VI} and one electron reduction to M^{IV}. It seems W^{V} is oxidized with more ease and reduced with more difficulty than Mo^{V}.

A similar trend is observed for the reduction of ternuclear Mo^{IV} and W^{IV} complexes $[M_3(\mu_2\text{-}O)_3(\mu_3\text{-}O)(H_2O)_9]^{4+}$, in which three M atoms are connected with three μ_2-O^{2-} and one μ_3-O^{2-} to give a cubane-like structure with one missing vertex and nine terminal aqua ligands. The configuration of M is very much distorted octahedral. The one electron reduction potential measured by cyclic voltammetry is as follows indicating easier reduction of molybdenum.

$[Mo^{IV}_3O_4(H_2O)_9]^{4+}$	-0.341 V vs. S.C.E.	(ref. 18)	in p-toluene-sulphonic acid, 2 M in water
$[W^{IV}_3O_4(H_2O)_9]^{4+}$	-0.50 V "	(ref. 19)	

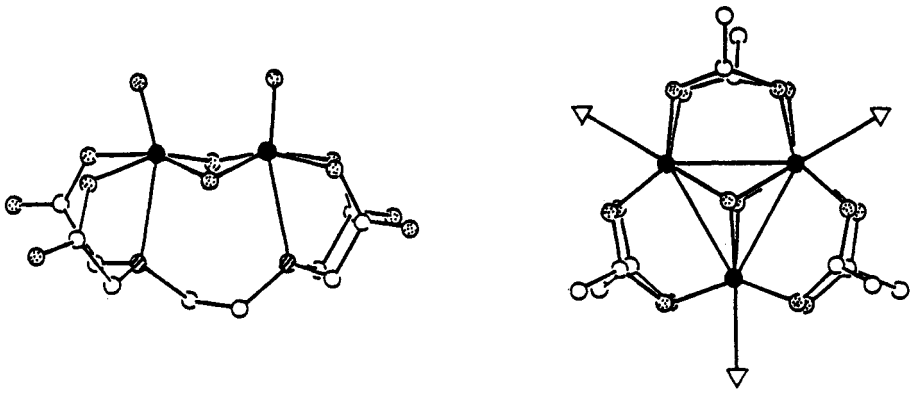

Fig. 7 Structure of $[Mo^{V}_{2}O_{4}(edta)]^{2-}$ (left) and ternuclear $[Mo^{IV}_{3}(\mu_3\text{-}O)_2(\mu_2\text{-acetate})_6(H_2O)_3]^{2+}$
o carbon, ● nitrogen, ⊛ oxygen, ● metal ion, Δ H_2O

Table 4 Electrode potentials of $[M^{V}_{2}O_{4}(edta)]^{2-}$ in aqueous solution

M_2	Mo_2	MoW	W_2
$M^{V}_{2} \rightarrow M^{V}M^{VI}$	+0.98	+0.56	+0.43
$M^{V}_{2} \rightarrow M^{IV}M^{V}$	-1.34	< -1.5	< -1.5

vs. S.C.E.; working electrode, glassy carbon; counter electrode, Pt; 25°C; I = 0.75 ($NaClO_4$); pH 7.5 (0.2 M phosphate buffer)

Table 5 Reduction potential of $[M^{IV}_{3}(\mu\text{-}O_3)_2(\mu\text{-acetate})_6(py)_3]Br_2$ in acetonitrile at 25°C.

M_3	I (rev)	II (rev)	III (irrev)
Mo_3	-0.08	-0.32	-0.86
Mo_2W	-0.07	-0.30	-1.25
MoW_2	-0.07	-0.32	-1.40
W_3	-0.08	-0.31	-1.45

V vs. $Ag/AgNO_3$(0.1 M) in 0.3 M $(C_4H_9)_4NClO_4$ in a mixture of acetonitrile and pyridine (4 + 1,v)

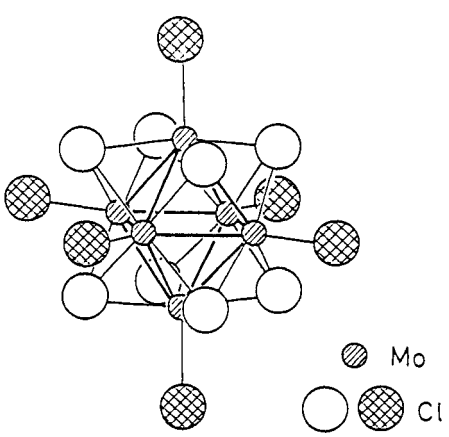

Fig. 8 Structure of cluster anion of $[(Mo_6Cl_8)Cl_6]^{2-}$ open circle, bridging hatched circle, terminal

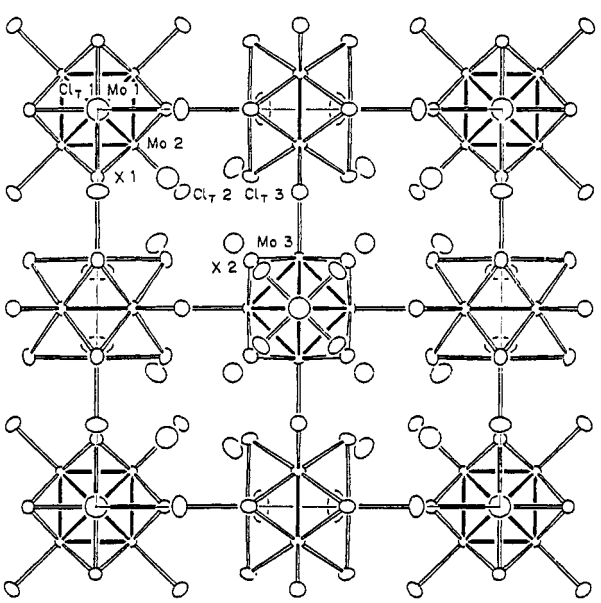

Fig. 9. Cubic lattice of the complex $Cs_2[(Mo_6Cl_6Se_2)Cl_6].9H_2O$. Mo_6 in 14+ state

Quadridentate molybdenum and tungsten also give ternuclear species bridged by two μ_3-oxides and six μ_2-acetates.(Fig. 7) Each metal atom has one terminal unidentate ligand e.g. H_2O and pyridine, and the structure is very distorted. Presence of interaction between metal atoms is suggested by the diamagnetism and the short M-M distance (2.7 Å for W-W). We have succeeded in the preparation of single crystals of mixed metal complexes with Mo_2W and MoW_2 cores, and determined the structure. (ref. 20) Electrode potantials of the full set of complexes with Mo_3, Mo_2W, MoW_2 and W_3 core in the form $[M_3(\mu_3\text{-}O)_2(\mu_2\text{-acetate})_6(py)_3]^{2+}$ are compared in acetonitrile containing 0.2 M $(C_4H_9)_4NClO_4$ and pyridine with hanging mercury, $Ag/AgNO_3$(0.1 M) and platinum electrode as working, reference and counter electrode, respectively. (Table 5) Aqua complexes in water are not useful for cyclic voltammetry.

In the region 0 to -1.6 V vs. Ag/Ag^+ electrode three waves are observed. Reversible first and second waves remain unchanged throughout the four complexes but the third irreversible wave shifts towards more negative side on the replacement of Mo by W. Assignment of the waves to individual redox process is uncertain at present. The trend towards more difficult reduction is, however, seen on going from Mo_3 to W_3 species, and this is in accord with the reduction of other complexes with $[M^{V}_2O_4]^{2+}$ and $[M^{IV}_3O_4]^{4+}$ cores.

HEXAMOLYBDENUM CLUSTERS WITH MIXED CAPPING LIGANDS

Molybdenum atoms gather to form Mo_6 clusters with octahedral configuration, and the faces are capped with halides or chalcogenide ions to give $[Mo_6X_8]^{4+}$ or $[Mo_6Y_8]^{4-}$ core. The formers have terminal halides to give $[(Mo_6X_8)X_6]^{2-}$ complexes. (Fig. 8) Their salts are soluble in water or organic solvents and exhibit remarkable fluorescence. The electron transfer reactions take place with much difficulty and are observed only as quecking of the luminescence at room temperature. (ref. 21) On the other hand, those clusters capped by chalcogenides form solid compounds insoluble in any kind of solvent. Their electrons are, however, removed from the cluster very easily, so that a variety of non-stoichiometric compounds such as $Cu_xMo_6S_y$ and $Pb_xMo_6Se_y$ have been synthesized. Some of them are super-conductors (Chevrel-type compounds). (ref. 22)

Such a marked difference in electron transfer from the Mo_6 core must originate from the variety of capping ligand. However, only little is known concerning the mixed capping ligand complexes. McCarley and Michel (ref. 23) synthesized pyridinium salt of $[(Mo_6Cl_7S)Cl_6]^{3-}$ and determined the crystal structure, but the chemical properties in solution remains unknown.

We have synthesized a variety of mixed capping ligand complexes in the form of single crystals, determined the crystal structures, and measured their properties in solution, particularly the electrochemical behavior by cyclic voltammetry. Crystals with oxidized forms of the clusters were also obtained as single crystals and the bond distances within the cluster were compared with the original complexes. (The oxidation state of the cluster is expressed by the formal charge number of Mo_6 core for convenience.)

A mixture of $MoCl_2$, NaHS (or NaHSe) and pyridine were refluxed and the products were submitted to ion exchange and gel permeation chromatography with Dowex 50W and Sephadex LH-20, respectively. The complex with $[Mo_6Cl_6Se_2]$ core with Mo_6 in 12+ state gave two fractions on elution from Dowex 50W column with 0.1 to 0.3 M H_2SO_4; red (A) solution is eluted earlier than orange solution (B), both having aqua ligands at the terminal sites. They are coverted into $[(Mo_6Cl_6Se_2)Cl_6]^{4-}$ in hydrochloric acid. They seem to consist of geometrical isomers in which the location of two capping selenides is different. Each of A and B complexes can be oxidized to give 13+ and 14+ state of Mo_6 core.

Caesium salts gave good single crystals for X-ray diffraction studies, and tetrabutylammonium salt for cyclic voltammetry in acetonitrile. Aqueous solution is not useful for CV studies, because the terminal ligand changes easily. Table 6 and 7 summarize the result, and Fig. 9 shows the unit cubic lattice of $Cs_2[(Mo_6Cl_6Se_2)Cl_6].9H_2O$ (Mo_6 in 14+ state, isomer A).

Capping halide and chalcogenide ions are disordered in all the crystals of the composition (Mo_6X_7Y) and $(Mo_6X_6Y_2)$. The geometrical isomers are not distinguished from each other by the crystal analysis of the latters.

TABLE 6 Structural data of hexamolybdenum cluster complexes with mixed capping ligands and terminal chloride.

Compounds	Mo_6	I	SG	Mo-Mo	Mo-X_b	Mo-Cl_t
1. $Cs_3[(Mo_6Cl_7S)Cl_6].H_2O$	+12		$P\bar{1}$	2.609(2)	2.478(2)	2.467(6)
2. $Cs_3[(Mo_6Cl_7Se)Cl_6].H_2O$	+12		$P\bar{1}$	2.612(2)	2.500(2)	2.473(6)
3. $Cs_4[(Mo_6Cl_6Se_2)Cl_6].H_2O$	+12	A	$P6_3/mcm$	2.612(8)	2.515(6)	2.481(7)
4. $Cs_4[(Mo_6Cl_6Se_2)Cl_6].H_2O$	+12	B	$P6_3/mcm$	2.603(7)	2.506(6)	2.472(7)
5. $Cs_3[(Mo_6Cl_6Se_2)Cl_6].H_2O$	+13	B	$P\bar{1}$	2.641(8)	2.523(6)	2.481(15)
6. $Cs_2[(Mo_6Cl_6Se_2)Cl_6].9H_2O$	+14	A	Pm3m	2.622(4)	2.518(6)	2.516(10)
7. $Cs_2[(Mo_6Cl_6S_2)Cl_6].9H_2O$	+14	M	Pm3m	2.618(8)	2.480(5)	2.490(10)
8. $(pyH)_3[(Mo_6Cl_7S)Cl_6]$	+12		$P2_1/c$	2.604(2)	2.473(4)	2.454(4)

Mo_6: formal charge number of Mo_6 cluster. I: isomers, see text, M, mixture. SG: space group. pyH: pyridinium ion, ref. 23.

TABLE 7 Electrode potential of hexamolybdenum cluster complexes with mixed capping ligands and terminal halide.

Complexes [a]		+14/+13 [b]	+13/+12 [b]	+12/+11 [b]
1.	$[(Mo_6Cl_8)Cl_6]^{2-}$	irrev. [c]	+1.56 [c]	-1.53 [c]
2.	$[(Mo_6Br_8)Br_6]^{2-}$	——	+1.38	< -1.7
3.	$[(Mo_6Cl_7S)Cl_6]^{3-}$	> +1.4	+0.69	< -1.7
4.	$[(Mo_6Cl_7S)Br_6]^{3-}$	> +1.4	+0.74	< -1.7
5.	$[(Mo_6Cl_7Se)Cl_6]^{3-}$	> +1.4	+0.64	< -1.7
6.	$[(Mo_6Br_7S)Cl_6]^{3-}$	> +1.3	+0.55	< -1.7
7.	$[(Mo_6Cl_6Se_2)Cl_6]^{4-}$ (A)	+0.51	-0.24	< -1.7

In acetonitrile, against Ag/Ag^+ (0.1 M $AgNO_3$) electrode, working electrode, glassy carbon; counter electrode, platinum; in $(C_4H_9)_4NClO_4$ (0.1 M)

a) Complexes in the form of $(C_4H_9)_4N^+$ salt, charges are of the Mo_6 (12+) state.

b) Charge numbers are those of Mo_6 clusters.

c) Potential data are converted into those against S.C.E., V.

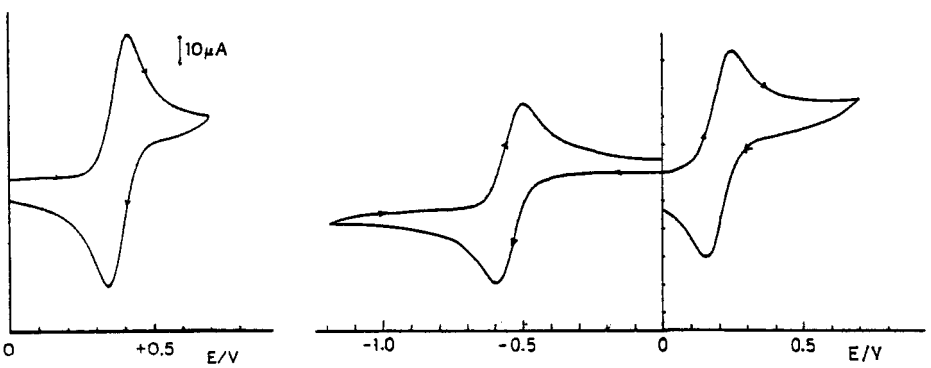

Fig. 10 Cyclic voltammograms of $[(C_4H_9)_4N]_3[(Mo_6Cl_7S)Cl_6]$ (left) and $[(C_4H_9)_4N]_4[(Mo_6Cl_6Se_2)Cl_6]$ (right) in acetonitrile. Glassy carbon, platinum and Ag/Ag^+ electrode in 0.1 M $(C_4H_9)_4NClO_4$, scanning rate 100 mV/s

Individual clusters in the single crystals may consist of a particular geometrical isomer, but orient irregularly in the lattices to result in disorder. Hence the Mo-capping ligand distances (Mo-X_c) are reckoned as weighed mean of seven Mo-X and one Mo-Y, or six Mo-X and two Mo-Y distances.

It is remarkable to find that the distances Mo-Mo, Mo-X_c and Mo-Cl_t do not differ much among the listed compounds, despite the fact that the kind of capping ligand and the oxidation state of Mo_6 moiety are widely different. Most marked difference in properties among the compounds is seen in the redox behavior on electrodes. (Fig. 10, Table 7) Substitution of one chalcogenide for the capping halide brings about the decrease of oxidation potential by ca. 0.9 V, corresponding to ca. 80 kJ mol^{-1}. The change due to the replacement of the terminal chlorides by bromides is very modest. (ca. 0.05V) In good contrast to the big difficulty with which $[(Mo_6Cl_8)Cl_6]^{2-}$ (Mo_6 in 12+ state) undergoes electron transfer reactions, the complexes with mixed capping ligand are not only oxidized with much lesser difficulty, but even the oxidized complexes give stable crystals to enable X-ray crystallography and cyclic voltammetry.

This fact may be due to the nature of the Mo_6 core. Not only $(Mo_6)^{12+}$ but also $(Mo_6)^{14+}$ are diamagnetic, and only $(Mo_6)^{13+}$ species in tetrabutylammonium salt gave ESR signals in chilled acetonitrile and methanol containing hydrogen chloride. The valence electrons in the Mo_6 moiety should be very delocalized. Studies by ESR spectroscopy of the $(Mo_6)^{13+}$ complexes as well as of other diamagnetic complexes on irradiation with laser light will provide useful information. Even one or two capping halide ions by chalcogenide causes a marked difference in electron transfer reaction to approach the state of Chevrel type compounds with octachalcogenide capping ligands.

Acknowledgement The authors are very grateful to our colleagues, whose names are in the reference lists, particularly Dr. M.Nishizawa and Messrs. B.-T. Wang and M.Ebihara for useful cooperation. They are also indebted to the Ministry of Education, Science and Culture of Japanese Government for Grant-in-Aid.

REFERENCES

1. K.Saito, *Coordination Chemistry-20*, (Pergamon Press, Oxford, 1980)173-181
2. M.Nishizawa and K.Saito, *Inorg. Chem.*,17, 3676-3679 (1978).
3. M.Nishizawa and K.Saito, *Bull. Chem. Soc. Jpn.*, 53, 664-667 (1980).
4. M.Nishizawa and K.Saito, *Inorg. Chem.*, 19, 2284-2288 (1980).
5. M.Nishizawa, K.Hirotsu, S.Ooi and K.Saito, *J. Chem. Soc., Chem. Commn.*, 1979, 707-708.
6. H.Taguchi, K.Isobe, Y.Nakamura and S.Kawaguchi, *Buul. Chem. Soc. Jpn.*, 51, 2030-2034 (1978).
7. Y.Sasaki, M.Kanesato, K.Okazaki, A.Nagasawa and K.Saito, *Inorg.Chem.*, 24, 772-775 (1985).
8. A.Kojima, K.Okazaki, S.Ooi and K.Saito, *Inorg. Chem.*, 22, 1168-1174(1983).
9. B.-T.Wang, Y.Sasaki, K.Okazaki, K.Kanesato and K.Saito, *Inorg. Chem.*, 25, 3745-3749 (1986).
10. M.Nishizawa, Y.Sasaki and K.Saito, *Inorg. Chem.*, 24, 767-772 (1985).
11. A.Bakac, R.Marcec and M.Orhanovic, *Inorg. Chem.*, 16, 3133-3135 (1977).
12. Y.Sasaki and K.Saito, unpublished.
13. Y.Sasaki, *Bull.Chem.Soc.Jpn.*,50 1939-1944 (1977).
14. S.Kondo, Y.Sasaki and K.Saito, *Inorg. Chem.*, 20, 429-433 (1981).
15. Y.Sasaki, K.Meguro and K.Saito, *Inorg. Chem.* 25, 2277-2278.
16. Z.Dori, *Prog. Inorg. Chem.*, 28, 239-307 (1981).
17. S.Ikari, Y.Sasaki, A.Nagasawa and T.Ito, unpublished.
18. D.T.Richens and A.G.Sykes, *Inorg. Chem.*, 21, 418-422 (1982).
19. M.Segawa and Y.Sasaki, *J. Amer. Chem. Soc.*, 107, 5565-5566 (1985).
20. B.-T. Wang, Y.Sasaki, A.Nagasawa and T.Ito, *J. Amer. Chem. Soc.*, 108, 6059-6060 (1986).
21. H.K.Tanaka, Y.Sasaki and K.Saito, *Sci. Papers Inst. Phys. Chem. Res.*, 78, 92-97 (1984).
22. K.Yvon, *Current Topics in Material Science*, E.Kaldis Ed., (North Holland, 1978) Vol. 3 Chapter 2.
23. R.E.McCarley and J.B.Michel, *Inorg. Chem.*, 21, 1864-1872 (1982).
24. M.Ebihara, K.Toriumi and K.Saito, in preparation.
25. M.Ebihara, K.Toriumi and K.Saito, unpublished.